Geomechanics and Engineering, Vol. 2, No. 2 (2010) 107-123
DOI: http://dx.doi.org/10.12989/gae.2010.2.2.107

Assessment of long-term behaviour of a shallow tunnel in clay till

Z. Wang[1], *R.C.K. Wong[1] and H. Heinz[2]

[1]*Department of Civil Engineering, Schulich School of Engineering, The University of Calgary, 2500 University Drive NW, Calgary, Alberta, Canada*
[2]*Thurber Engineering Limited, Calgary, Alberta, Canada*

(Received February 13, 2010, Accepted June 14, 2010)

Abstract. Ground settlements and pore pressure changes were monitored around a shallow tunnel constructed in clay till during the excavation and primary lining installation. The settlements above the tunnel continued to develop for up to 100 days after the primary lining installation. Triaxial compression tests were carried out to estimate the short-term and long-term deformation characteristics of the till. Numerical simulation was conducted to history match the field measurements, and thus, to quantify the settlements induced by ground stress relief, consolidation and creep. It was found that the surface settlements due to ground stress relief, consolidation and creep are 17, 12 and 71% of total settlement (about 44 mm), respectively. In addition, early installation of rigid concrete lining could be an effective means to reduce the settlement due to creep.

Keywords: shallow tunnel; clay till; consolidation; creep; settlement.

1. Introduction

The construction of a tunnel in soft ground generally induces short-term and long-term ground settlements above the tunnel. The short-term ground settlements are mainly caused by the relief of in-situ ground stress (Peck 1969, Wong and Kaiser 1991). For the long-term ground settlements above tunnels, most of the existing studies interpreted them in terms of consolidation theory, in which the grounds were considered as elastoplastic materials (Lee and Rowe 1991, Shin *et al.* 2002, Shin and Potts 2003, Karakus and Fowell 2003, Wongsaroj *et al*. 2007, Mair 2008). However, soft soils exhibit pronounced creep deformation. It is widely accepted that creep deformation influences the long-term responses of soil, such as settlement of ground and movement of slopes. Therefore, it is of practical significance to assess the long-term ground settlements above tunnels buried in soft grounds in the manner that creep of ground is taken into consideration.

In this study, the long-term ground settlements above Shepard tunnel were numerically assessed. The unique aspect of the tunnel is that it crosses the in-operation Canadian Pacific Railway (CPR). There were numerous requirements that needed to be met before the CPR would allow the construction to take place. One of the requirements was that the final surface settlement above the

*Corresponding author, Professor, E-mail: rckwong@ucalgary.ca

tunnel must be within an acceptable limit to the CPR criteria. Therefore, a field monitoring program was carried out during the construction of the tunnel. It was observed that significant components of surface and subsurface ground settlements developed after the primary lining was fully installed. Although a preliminary study using empirical method was conducted (Woytiuk *et al.* 2008, Heinz *et al*. 2008), a comprehensive study is still required to estimate the long-term ground settlements above the tunnel. This comprehensive study could benefit the future design and construction of tunnels in similar grounds.

2. Site characterization

The Shepard tunnel was constructed to divert storm water from a catchment area of 6,200 hectares in the Northeast quadrant of Calgary, Alberta, Canada to a new wetland treatment facility near the east boundary of the city. Fig. 1 shows the oblique aerial photograph of Shepard tunnel. The tunnel is 63 m long, 4 m wide and 4 m high. The tunnel alignment is nearly perpendicular to the railway. Fig. 2 shows the cross section and lining system of the tunnel. The primary support system consists of steel ribs and wood lagging. The permanent support system is made of cast-in-place concrete. The internal diameter of the concrete conduit is 3 m. Fig. 3 depicts the soil stratigraphy along the tunnel centerline, layout of the instrumentation for field monitoring, and tunnel construction method. The soil strategraphy shown in this Figure was recorded during the excavation. The surficial soil deposit in site consists of Crossfield formation till and Porcupine Hills formation bedrock. In some areas, the Crossfield formation is underlain by the Balzac formation or the Lochend formation till. The tills were deposited during sequences of advance and retreat of the last continental ice-sheet from the northeast (Moran 1986). Close to the project area, the origin of the till material is super glacial mudflow sediment with a morphology described as undulating to hummocky glacial-collapse terrain. A recent study indicated that the tills are moderately overconsolidated (Adams *et al.* 2008). The formation may contain isolated bodies of poorly sorted ice-contact fluvial channel sediments. The bedrock in the project area consists of interbedded

Fig. 1 Oblique aerial photograph of tunnel location (Heinz *et al.* 2008)

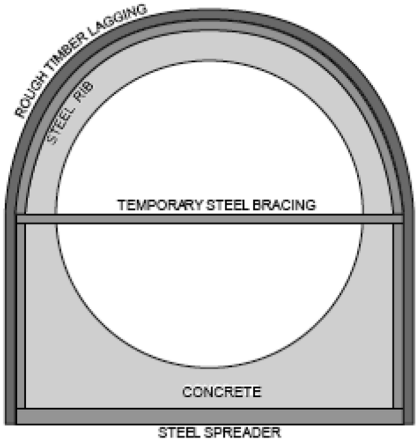

Fig. 2 Cross section of Shepard tunnel (Woytiuk *et al.* 2008)

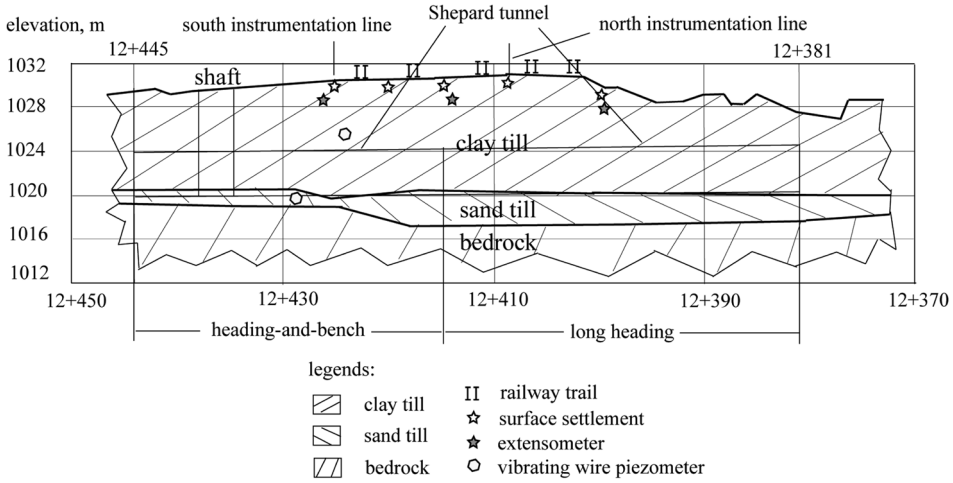

Fig. 3 Soil stratigraphy along the tunnel centerline and field instrumentation

sandstones, siltstones and claystones of Upper Cretaceous age.

3. Tunnelling method

The tunnel was excavated by hands. In the first phase of construction, a 4.6 m diameter shaft was excavated, which was located 7.75 m from the south end of the tunnel (Fig. 3). The excavation first advanced north, towards the CPR, and then to the south. Initially the heading and bench were advanced together, *i.e.*, heading-and-bench method. With this method, the advance rate of tunnel face was about 1 m/day. This tunnel face (TF) advance method was modified when a small crown cave-in happened during a shift at a section where the bench was being advanced. It was then decided that the heading would be advanced to the north end of the tunnel and the bench would be advanced once the upper bench was completed, *i.e.*, long heading TF advance method. With this method, the advance rates of heading and bench were about 2 m/day, respectively. The modification of TF advance method took place at about 21 m advancement from the shaft (Fig. 3). After the north segment of tunnel was all excavated, the tunnel was then advanced the final 7 m south of the shaft.

Steel ribs and wood or steel laggings were installed as primary support. W100 × 19 steel ribs were used at the crown and sidewalls of the tunnel. Steel bracing was used for temporary support after the excavation of heading. A W150 × 37 steel horizontal spreader was used at the tunnel's permanent invert. Cast-in-place concrete was used as permanent lining.

Different primary lining systems were used in sections below and outside the CPR, respectively. Wood lagging and steel ribs with a spacing of 1 m were used in sections outside of the right way of CPR. The spacing was reduced to 0.6 m and the steel laggings were used in sections below the right way of CPR. This measure was taken to limit the surface settlement above the tunnel in an allowable range.

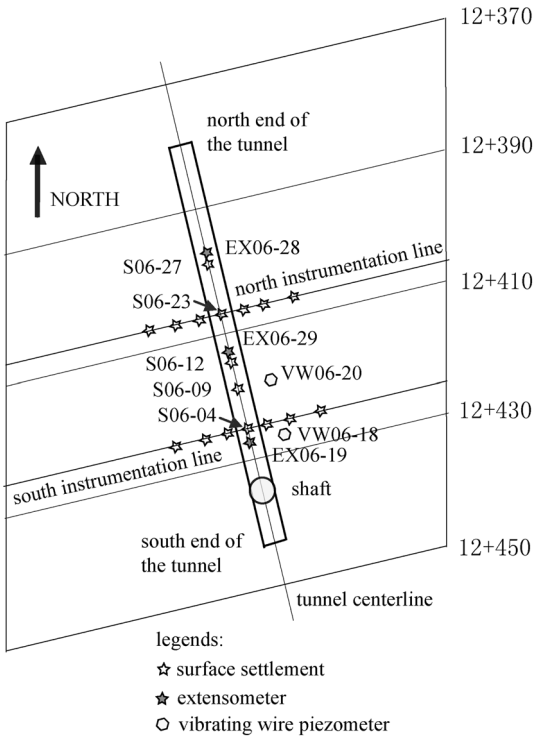

Fig. 4 Plan view of field instrumentation

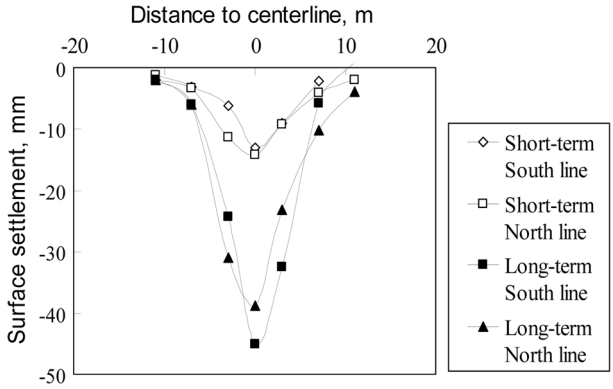

Fig. 5 Short-term (10 days) and long-term (100 days) surface settlement troughs above Shepard tunnel

4. Field monitoring

Various instruments were installed before the construction of the tunnel to monitor ground movements and groundwater response. Fig. 4 shows the plan view of the instrumentation. Further details can be found in Woytiuk (2008).

Totally 17 surface settlement monitoring points were installed before the excavation of the tunnel (Fig. 4). Among them, five points (S06-04, S06-09, S06-12, S06-23 and S06-27) spread out approximately every 5 m along the tunnel centerline. Other 12 points were installed along two instrumentation lines: south and north, where monitoring points S06-04 and S06-23 were installed, respectively. It should be noted that the tunnel sections at the south and north instrumentation lines were excavated using the heading-and-bench and long heading TF advance methods, respectively (see Fig. 3). Three benchmarks were installed in the bedrock, about 12 m away from the tunnel centerline. The monitoring of surface settlements was carried out using a digital level.

The excavation of the tunnel started on January 9, 2007 and completed on March 21, 2007. Fig. 5 shows the short-term and long-term surface settlement troughs measured at the south and north instrumentation lines. The short-term settlement troughs were measured when the TF advanced 2.5 times of tunnel diameter beyond the instrumentation lines, *i.e.*, 10 m. With the advance rate of 1 m/day, the short-term settlement trough measurements were taken at about 10 days after the excavation of the sections below the instrumentation lines. The long-term settlement troughs were measured at

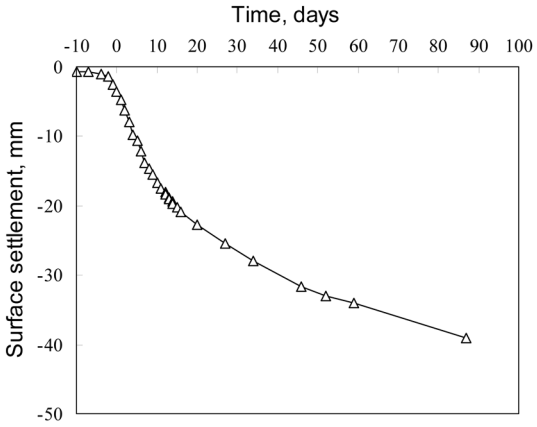

Fig. 6 Surface settlement versus time relation at monitoring point S06-04

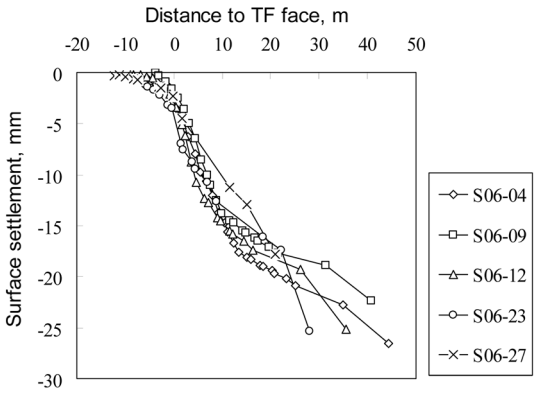

Fig. 7 Surface settlement versus distance to TF relations for monitoring points along tunnel centerline

about 100 days after the TF advanced well beyond the instrumentation lines and when the concrete liner was cast.

Fig. 6 plots the surface settlement against time relation at the monitoring point S06-04, under which the section of tunnel was excavated with heading-and-bench TF advance method. Fig. 7 shows the surface settlement versus distance to TF relations for the monitoring points along the tunnel centerline. The heading-and-bench TF advance method was used at the sections below the settlement points of S06-04, S06-09 and S06-12, whereas the long heading TF advance method was used at the sections below the settlement points S06-23 and S06-27. From Figs. 5 and 7, it appears that the employment of long heading TF advance method reduced the short-term settlements as observed at the settlement point of S06-23, and long-term settlements as observed along the north instrumentation line. However, the monitoring data are insufficient to draw this conclusion.

Spider type extensometers were installed to monitor subsurface settlements. Three sets of extensometers were installed directly above the tunnel crown. Each set consisted of three spider magnets installed approximately 1.5 m above the tunnel crown. The depth measured was based on the top of the access pipe. Since the top of the pipe was assumed to settle at the same rate as the ground surface, the settlements measured at the extensometer were added to the settlement measured at the nearest surface settlement monitoring point.

Among three sets of extensometers, EX06-19 showed consistent and reliable reading over the entire period of the tunnel construction. Fig. 8 shows the subsurface settlement versus distance to TF relations at the extensometer EX06-19. From Figs. 6, 7 and 8, only a small percentage of settlements occurred ahead of the TF, and approximately 65% of the surface settlements and 85% of the subsurface settlements took place when the TF was advanced a distance of 2.5 times of tunnel diameter (*i.e.*, 10 m) beyond the instrumentation lines. The continued settlements would be caused by the creep behaviour of the till.

Open well standpipes and vibrating wire piezometers were installed in the ground during the construction. Among them, two vibrating wire piezometers (VW06-18 and 06-20) were installed near the south instrumentation line to monitor the effect of the tunnel construction on groundwater, while the others were installed to monitor the effect of shaft construction on groundwater.

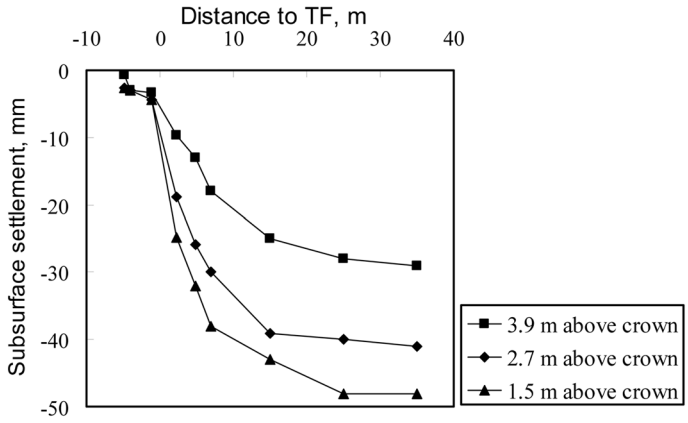

Fig. 8 Subsurface settlement versus distance to TF relations at extensometer EX06-19

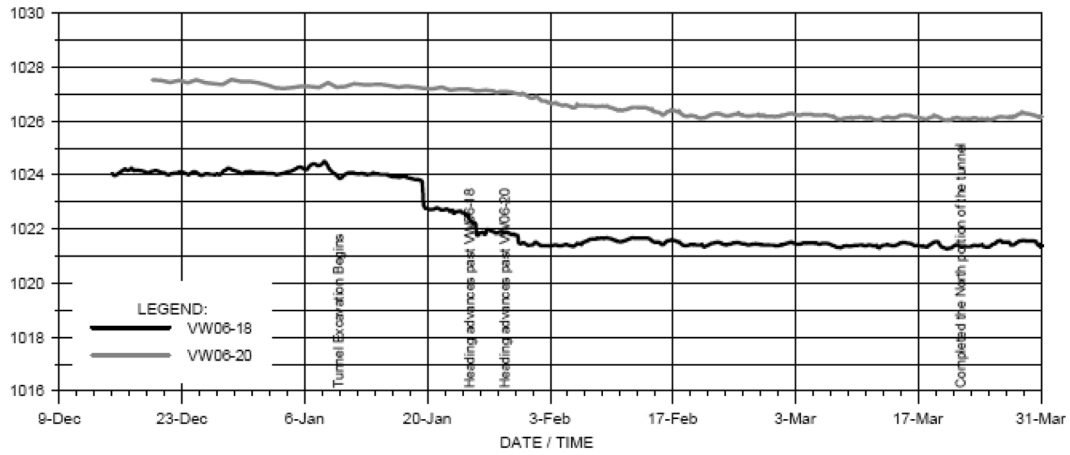

Fig. 9 Groundwater responses at piezometers VW06-18 and VW06-20 (Woytiuk 2008)

Fig. 9 shows the groundwater responses due to the construction of the tunnel measured at the piezometers VW6-18 and VW6-20. A relative scale was used in the vertical axis of Fig. 9 for illustration clarity. During the tunnel excavation and primary lining installation, changes in pore pressure head of about 2.5 and 1.5 m (25 and 15 kPa) were observed at the piezometers VW6-18 and VW6-20, which occurred over periods of 14 and 28 days, respectively. The pressure drops reacted consistently with the tunnel advance rate. The pore pressure heads in both piezometers remained steady after the excavation, indicating a steady water flow into the tunnel. Thus, the primary lining composed of steel ribs and wood or steel lagging was permeable.

5. Numerical simulation

Fig. 10 depicts the configuration of the problem. It is composed of two formations, *i.e.*, the 12 m thick clay till and the 8 m thick bedrock formations. The influence of sand till is not considered

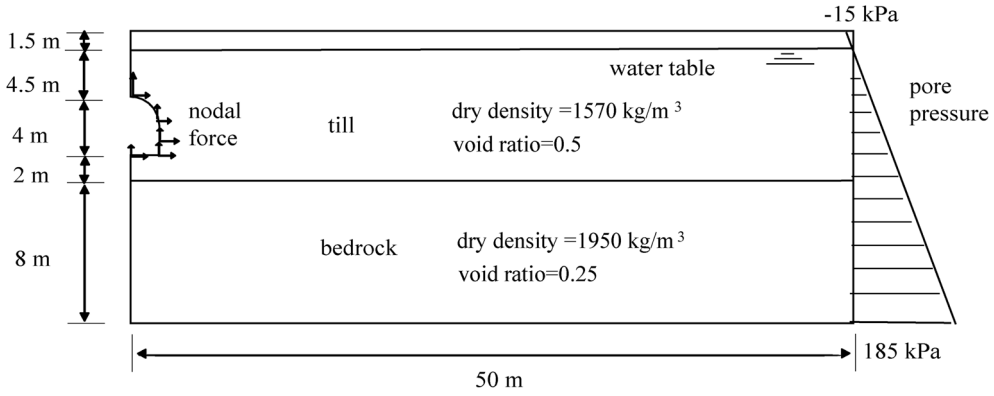

Fig. 10 Configuration of the problem

owing to its limited volume around the tunnel. The initial groundwater table is 1.5 m below the ground surface. The initial vertical effective stress was calculated by integrating from the self-weights of different formations. The ratio of in-situ effective horizontal stress to vertical stress (K_o) was assumed to be 0.7. According to field and laboratory measurements, the dry densities of till and bedrock are about 1570 kg/m^3 and 1950 kg/m^3, respectively, and the initial void ratios of till and bedrock are about 0.5 and 0.25, respectively.

Tunnel construction involves removal of ground and installation of a support system. The removal of ground induces a ground stress relief and redistribution around the tunnel opening, resulting in a decrease in radial stress and an increase in tangential stress at tunnel wall. The installation of the support system provides some internal support stress around the tunnel periphery. The change in ground stresses induces the ground settlements above the tunnel. The higher the ground stress relief, the higher the ground settlements are. However, if the ground is characterized with creep behaviour, ground settlements develop with time, even without further relief of ground stress.

When groundwater flow is taken into consideration, a coupled pore pressure/stress, *i.e.*, consolidation analysis, is always used to model the interaction of ground deformation and groundwater flow. In a coupled pore pressure/stress analysis, change in pore pressure generates deformation, and at the same time, volumetric change causes change in pore pressure. In this study,

Fig. 11 2D finite element mesh and layout of trace lines

the coupled problem was solved using a commercial code, ABAQUS (2006). This code considers a permeable soil as a porous medium and adopts the principle of effective stress in analysis.

A wide mesh was adopted in the simulation to reduce boundary effects. Fig. 11 shows the finite element mesh and the layout of the trace lines. The width and height of the mesh are 50 m and 20 m, respectively. The mesh consists of 2105 8-node biquadratic, reduced integration plane strain elements, hybrid with linear pressure. Only half of the formation was simulated due to symmetry of the problem. No vertical displacements were allowed along the base of the mesh, and no lateral displacements were allowed along the vertical sides of the mesh, and the top surfaces of the mesh were allowed to deform freely. No fluid flow was allowed along the symmetry axis and at the base of the mesh. Hydrostatic pore pressure condition was applied at the far right side of the mesh.

For simulating excavation and lining installation, following steps were adopted:

1. Establish the initial stress field by applying the gravity stress and specifying the ratio of in-situ effective horizontal to vertical stresses.
2. Remove elements inside the tunnel and reinstate the initial stresses by applying equivalent nodal forces around the tunnel periphery.
3. Simulate the tunnel excavation and tunnel advance face effect by proportionally reducing the nodal forces around the tunnel periphery at a constant rate equal to the excavation rate. The percentage of ground stress relief, *i.e.*, 50% in this study, is obtained by history matching the field settlement data.
4. Simulate the installation of primary (permeable) lining by applying the support stress and controlling the flow condition at the tunnel periphery.
5. Allow the ground to consolidate and creep for specified periods of time, considering the clay till as an elastoplastic or elastic-viscoplastic material.
6. Simulate the installation of the permanent concrete lining by restraining the nodal displacement around the tunnel periphery.

Table 1 lists the material parameters for different formations. These values were estimated based on test results from drained triaxial compression tests (Wang 2010) and previous experience (Heinz

Table 1 Model parameters for till and bedrock (all geotechnical properties are drained parameters)

Properties	Till	Bedrock
Dry density (kg/m^3)	1570	1950
Void ratio	0.5	0.25
Horizontal permeability (m/s)	2×10^{-9}	2×10^{-11}
Vertical permeability (m/s)	4×10^{-10}	2×10^{-11}
Young's modulus (MPa)	20	300
Poisson's ratio	0.4	0.35
DP friction angle	29º	–
(MC friction angle)	(18º)	–
Dilation angle	0	–
DP cohesion (kPa)	200	–
(MC cohesion)	(119)	–
Creep coefficient A_t	3.42×10^{-11}	–
Creep coefficient n_t	0.94	–
Creep coefficient m_t	–0.39	–

et al. 2008) in the Calgary area. The bedrock was assumed to be an elastic material. The till is medium brown in color, and consists of approximately 30 to 50% sand, 30 to 40% silt and 20 to 30% clay. The water content of the till is about 19.2%. The liquid and plastic limits were determined to be 33.4 and 15.0%, respectively. The till displays anisotropy in permeability.

Extended Drucker-Prager (DP) model, *i.e.*, perfectly elastic-viscoplastic model was used to quantify the geotechnical properties of the till. The elastic properties are defined by the Young's modulus E, and the Poisson's ratio ν. The yield criterion of the model is given as

$$F = q - p' \tan \beta - c_{DP} = 0 \tag{1}$$

in which, p' and q are mean effective and deviatoric stresses, respectively, $\tan\beta$ is the slope of the yield surface in $p' - q$ plane, β is referred to as the friction angle of the soil, and c_{DP} is the cohesion of the soil.

The yield surface of this model is a circle on the deviatoric stress plane and is inscribed by the yield surface of Mohr-Coulomb (MC) model, which is an irregular hexagon on the deviatoric stress plane. Therefore, this extended DP model may underestimate the extent of the yield zone if yielding is developed around the tunnel, and thus the deformation of the till, as compared to those predicted by MC model.

For the same failure criterion in triaxial compression for the two models, the relation between the friction angle in this model and the friction angle in MC model is related as (ABAQUS 2006)

$$\tan\beta = \sqrt{3}\sin\phi \tag{2}$$

where ϕ is the friction angle in MC model. The relation between the cohesion in this model and that in MC model could be given as

$$\frac{c_{DP}}{c_{MC}} = \sqrt{3}\cos\phi \tag{3}$$

where c_{DP} and c_{MC} are the cohesions in this model and in MC model, respectively. For the case of $\phi = 18^{o}$ and $c_{MC} = 119$ kPa, $\beta = 29^{o}$ and $c_{DP} = 200$ kPa.

The plastic flow potential of the model is given as

$$G = q - p' \tan\psi \tag{4}$$

where ψ is the dilation angle. For a nondilational flow, the dilation angle is set to be zero. In this study, perfectly plastic model was used to describe the plastic behaviour of the till.

In the extended DP model, the creep behaviour is closely associated to the plasticity of material. The potential for plastic deformation is used to describe creep deformation, which is consistent with the experimental observations from Lade and Liu (1997). Therefore, Eq. (4) was also used to describe the creep flow of the till in this study.

The concepts of equivalent creep surface and equivalent creep stress are adopted in the model developed in ABAQUS (2006). The equivalent stress is determined as the intersection of the equivalent creep surface with the stress path in uniaxial compression test. In this manner, the magnitudes of the components of triaxial creep rate (a tensor) could be specified using the magnitude of an equivalent uniaxial compression creep rate (a scalar), along with the potential function. The creep rate in the model could be specified with a creep strain-version of time-dependent power law as

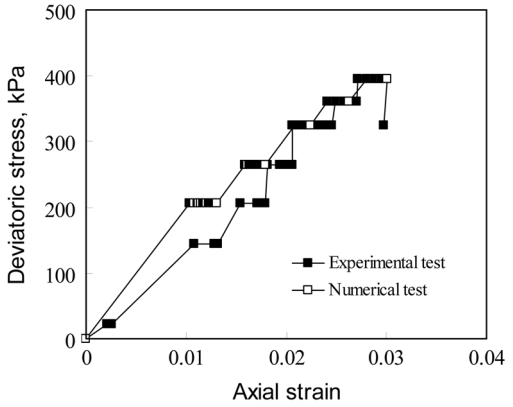

Fig. 12 Deviatoric stress versus axial strain relations of till in experimental and numerical tests

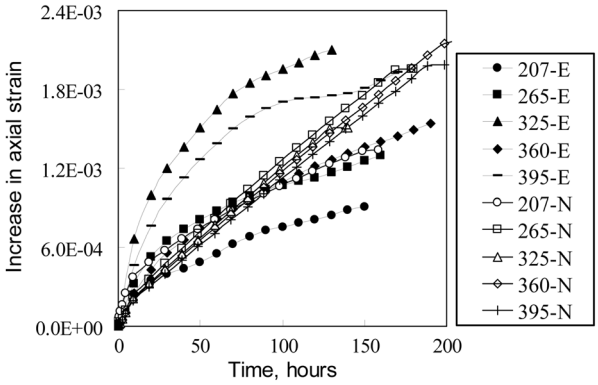

Fig. 13 Axial strain versus time relations of till in experimental and numerical tests ('E' and 'N' denote experimental and numerical test results, respectively)

$$\dot{\bar{\varepsilon}}^{cr} = (A_t(\bar{\sigma}^{cr})^{n_t}[(m_t+1)\bar{\varepsilon}^{cr}]^{m_t})^{\frac{1}{m_t+1}} \tag{5}$$

where $\bar{\varepsilon}^{cr} = \varepsilon_1^{cr}$ is the equivalent creep strain, $\bar{\sigma}^{cr} = (q - p\tan\beta)/(1-\tan\beta/3)$ is the equivalent creep stress, A_t, m_t and n_t are model parameters.

To model the response of the groundwater in the partially saturated till, the soil-water characteristic curves observed in clay till by Fredlund and Xing (1994) were used in the simulation. The saturation degree versus pore pressure relation was assumed to be linear. At zero pore pressure, the saturation degree is 1.0, while at the pore pressure of −200 kPa, the saturation degree is 0.9. The relation between the relative permeability and the saturation degree was also assumed to be linear. At the fully saturated state, the relative permeability is 1.0, while at the saturation degree of 0.9, the relative permeability is 0.9. Details of partially fluid flow theory could be found in other references (Fredlund and Rahardjo 1993).

Drained triaxial compression tests were carried out to determine the deformation and creep characteristics of till from cores recovered from the Shepard tunnel site (Wang 2010). Figs. 12 and 13 compare experimental results of a drained triaxial compression test (3D-TL-SW-100) with those from the extended DP elastic-viscoplastic model. The triaxial test was performed in two steps. In the test, the sample was allowed to consolidate for 2 days at an isotropic confining pressure of 100 kPa. Then, the sample was allowed to shear and creep at the specified deviatoric stresses in a sequence from low level to high level (207, 265, 325, 360 and 395 kPa). For each load increment, shear and creep deformations were separated using the concept of t_{100} consolidation (Wang 2010).

Fig. 12 compares the deviatoric stress versus axial strain relations of the till in the experimental (3D-TL-SW-100) and numerical element tests. Fig. 13 compares the axial strain versus time relations of the till in the experimental and numerical element tests. The model yields creep rates higher than those observed in the test. It should be noted that in this model, the direction of creep flow is specified by the dilation angle, and therefore there is no volumetric change in the creep stages in the numerical test (the dilation angle of the till is assumed to be zero). No excess pore

pressure would be generated during creep.

6. Results and discussions

A parametric study consisting of numerous simulations was conducted to investigate how different parameters including till geotechnical and hydraulic properties, tunnel advance face effect, drainage condition, primary and permanent support systems affect the behaviour of Shepard tunnel (Wang 2010). This paper only presents the cases which are considered to be "best-matched" or representative against the in-situ situation with the available data and knowledge (Table 1). Cases 1 and 2 involved coupled consolidation analyses without and with ground creep process, respectively.

Fig. 14 shows the predicted short-term surface settlement troughs in Cases 1 and 2, along with those from field monitoring. In the simulations, the permeable lining was simulated by setting zero pore pressure at the nodes at the tunnel periphery. In addition, the permeability of the primary lining was assumed to be 1×10^{-10} m/s which is relatively lower than to the anisotropic permeability of the till (Table 1, Mair 2008). This effect of primary lining permeability was simulated by adjusting the permeability of the finite elements around the tunnel periphery to the above value.

For the field monitoring, the term 'short-term' denotes the situation at that the tunnel face had advanced about 2.5 times of tunnel diameter (*i.e.*, 10 m) beyond the instrumentation lines. For the simulations, the short-term settlement trough denotes the settlement trough predicted at about 10 days based on the TF advance rate (*i.e.*, 1 m/day). To model the effect of the tunnel advance face, the internal support stress around the tunnel periphery was reduced from 100% to 50% of its in-situ stresses at a constant rate of 5% per day. The maximum short-term surface settlement (at center point) is about 9.0 mm in Case 1, while that is about 13.6 mm in Case 2. The difference in predicted surface settlements between Case 1 and Case 2 is attributed to the creep mechanism allowed during the tunnel excavation in Case 2. In Case 1, the settlement is mainly due to 50% ground stress relief and consolidation up to 10 days whereas in Case 2, the settlement is due to the combined effect of ground stress relief, consolidation and creep up to 10 days.

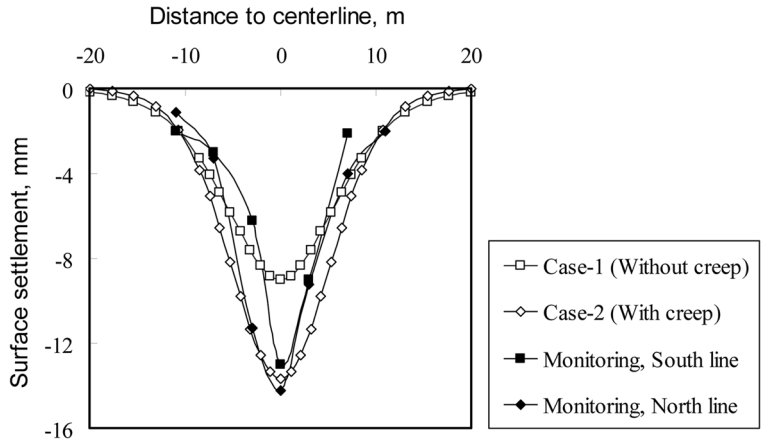

Fig. 14 Predicted short-term surface settlement troughs in Cases 1 and 2, along with those from field monitoring

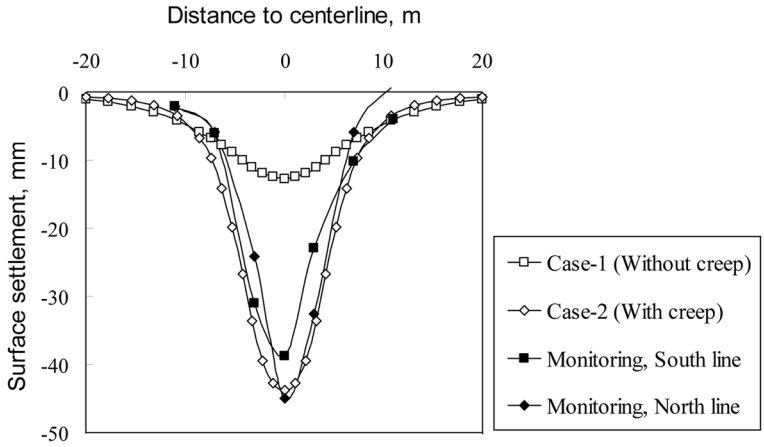

Fig. 15 Predicted long-term surface settlement troughs (100 days after the TF advanced beyond the instrumentation line) in Cases 1 and 2, along with those from field monitoring

Fig. 15 compares the predicted long-term surface settlement troughs in Cases 1 and 2. The 'long-term' settlements were estimated at 100 days after 50% ground stress relief. Under the condition of permeable lining, the maximum surface settlement (at the center point) after 100 days is 12.7 mm without taking the influence of ground creep into account (Case 1), while that is 43.7 mm taking the influence of ground creep into consideration (Case 2). For Case 1, the maximum surface settlement induced by consolidation occurred between 10 and 100 days is about 3.7 mm. The consolidation occurred in the till around the tunnel where groundwater was allowed to drain into the tunnel. The surface settlement induced by the 50% stress relief was estimated to be about 7.4 mm based on the simulation results obtained from a case study without consolidation analysis (Wang 2010). Results from Case 2 indicate that the creep behaviour of the ground plays a significant role in governing the long-term surface settlement above the tunnel. The creep settlement is about 71% of the total settlement.

The predicted short-term and long-term maximum surface settlements in Case 2 are consistent with those from field monitoring (Figs. 14 and 15). However, the simulation predicts settlement troughs wider than those observed in the field. Narrow trough could be simulated by use of low K_o coefficient and uneven support stress pattern (Wang 2010). In summary, Case 2 yields a case representative and close to the field situation based on the surface settlement assessment. This substantiates the use of 50% ground stress relief in simulating the excavation and primary support methods used in Shepard tunnel.

Fig. 16 shows the predicted surface settlement versus time relation at the monitoring point S06-24, along with those from field monitoring. The predicted result is consistent with that from field monitoring. This again verifies the use of 50% ground stress relief with 5% stress relief per day for modelling the construction method used in this particular case.

Among all the extensometers, EX06-19 showed reliable readings over the entire period of the construction of the tunnel, without any disturbance. The data obtained from this extensometer was herein used to compare with those from Case 2 in this study. Fig. 17 shows the predicted subsurface settlements versus time and subsurface settlement versus distance to TF relations at the extensometer, along with those from field monitoring. The predicted settlements above the crown

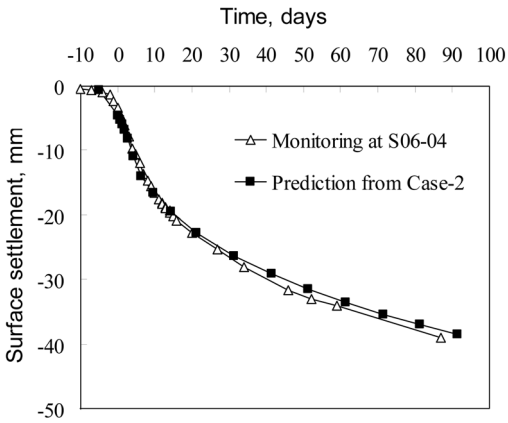

Fig. 16 Predicted surface settlement versus time relation at S06-04 in Case 2, along with that from field monitoring

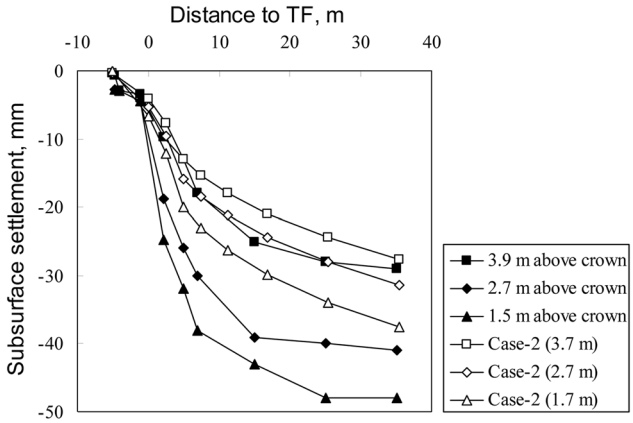

Fig. 17 Predicted subsurface settlement versus distance to TF relations at extensometer EX06-19 in Case 2, along with those from field monitoring

are less than those monitored. This discrepancy could be attributed to the fact that the till was assumed to behave linear elastic before plastic yielding. Non-linear elasticity might yield a better matching. The field data displays the 3D effect of the tunnel advance face. The soil reacted to the excavation and settled when the advanced face approached the monitored section at a distance of about 5 m or 1.25 times of diameter. This response could be simulated using 3D finite element models (Wang 2010).

Fig. 18 shows the predicted pore pressure changes at VW06-18 and VW06-20 in Case 2. The predicted magnitudes in pressure drop are consistent with the measured drops shown in Fig. 9. However, the field data shows that the drops occurred within 14-28 days after the primary lining installation and the pore pressure remained steady thereafter, supporting the consolidation induced by pore pressure drop developed within 14-28 days. The simulation predicts the pressure drop

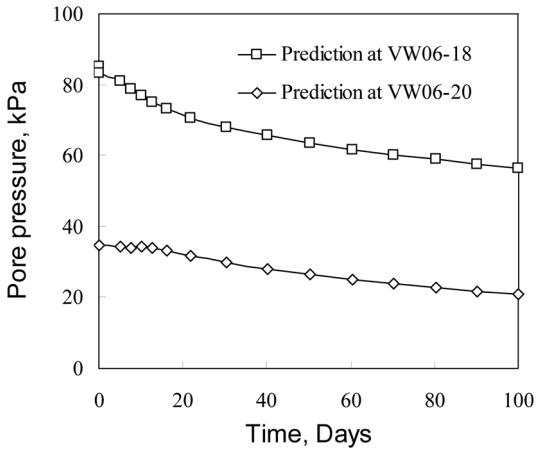

Fig. 18 Predicted pore pressure changes at piezometers VW06-18 and VW06-20 in Case 2

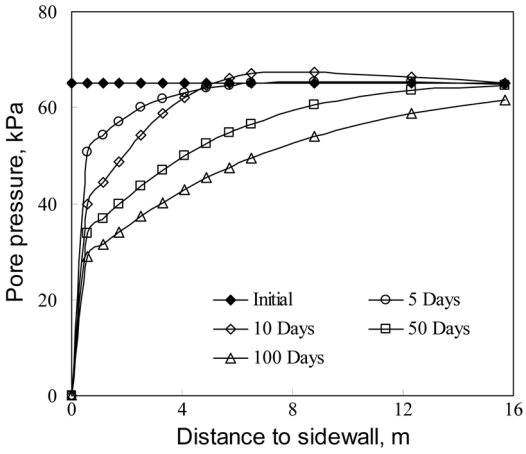

Fig. 19 Distributions of pore pressure at sidewall obtained in Case 2

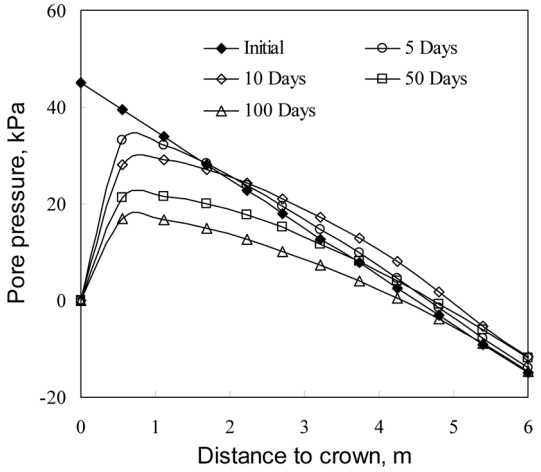

Fig. 20 Distributions of pore pressure above crown obtained in Case 2

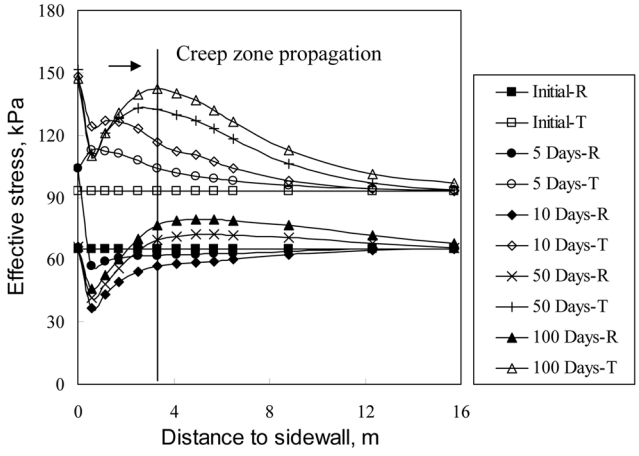

Fig. 21 Distributions of effective stresses at sidewall obtained in Case 2 ('R' and 'T' denote radial and tangential stresses, respectively)

developed over a longer period of time. This response could be explained by the fact that the sand till pockets were not included in the simulation.

Figs. 19 and 20 plot the distributions of pore pressure at the sidewall and above the crown in Case 2. The pore pressure is maintained at zero at the tunnel periphery during the excavation and primary lining installation and before the permanent concrete lining placement. These two figures show that the pressure drops induced by the groundwater table drawdown after 10 days or the advance face passed the monitored section became insignificant. There are small changes between 50 and 100 days. It will take a long period of time for the pore pressure to reach a steady state. It is of practical interest to notice that the unsaturated zone above the crown extended downward due to the groundwater table drawdown. The estimated average water inflow rate into the tunnel for the case of permeable lining is about 0.006 m^3/m/day.

Figs. 21 and 22 show the distributions of radial and tangential effective stresses at the sidewall and above the crown in Case 2. The 50% stress relief occurred over the first 10 days causes a total stress redistribution around the tunnel opening, resulting in a decrease in total radial (support) stress and an increase in total tangential stress. Drainage condition at the tunnel periphery causes the pore pressure drop to zero at the boundary, and thus the groundwater table drawdown. The combined effect of 50% stress relief and drainage produces similar trends in distributions of effective radial and tangential stresses at the sidewall as well as above the crown. After the first few days, the effective radial stress increases because the rate of pore pressure drop is higher than that of stress relief. The consolidation process dominates during this period. After the completion of 50% stress relief, the creep process starts to dominate. The effective radial stress decreases with time and creeps back to its initial state. All 3 mechanisms, the 50% stress relief, drainage and creep, cause increase in effective tangential stress. The magnitudes of the stress redistribution due to the 50% stress relief and pore pressure drop are larger than those due to creep. The stress redistributions illustrated in Figs. 21 and 22 indicate that no plastic yielding was induced by the 50% stress relief and pore pressure drop around the tunnel. However, the till started to creep at the sidewall and the

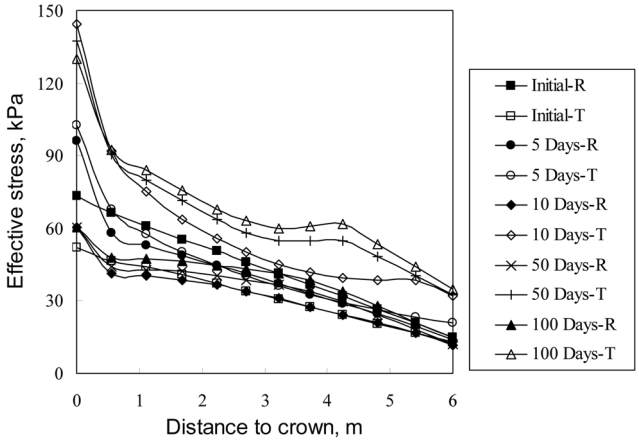

Fig. 22 Distributions of effective stresses above crown obtained in Case 2 ('R' and 'T' denote radial and tangential stresses, respectively)

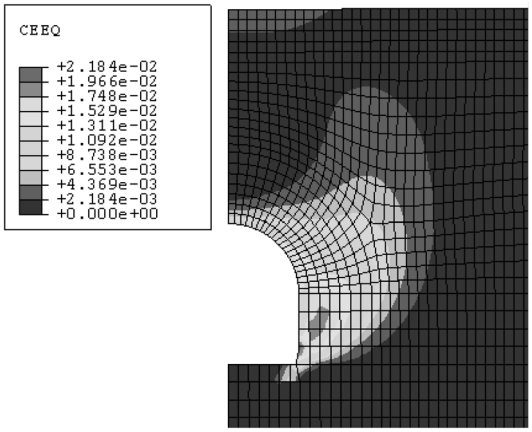

Fig. 23 Distribution of equivalent creep strains around tunnel ($t = 100$ days) obtained in Case 2

creep zone grows with time.

Fig. 23 shows the distribution of equivalent creep strains around the tunnel at 100 days obtained in Case 2. The equivalent creep strain (CEEQ) is defined as $\int \dot{\bar{\varepsilon}}^{cr} dt$ (ABAQUS 2006). The maximum equivalent creep strain is 0.022. The extent of creep zone is about 3.3 m away from the tunnel periphery at the sidewall, and the creep zone above the crown is less than 0.5 m. The configuration of the creep zone is very similar to the localized yielded zone of Mode I around

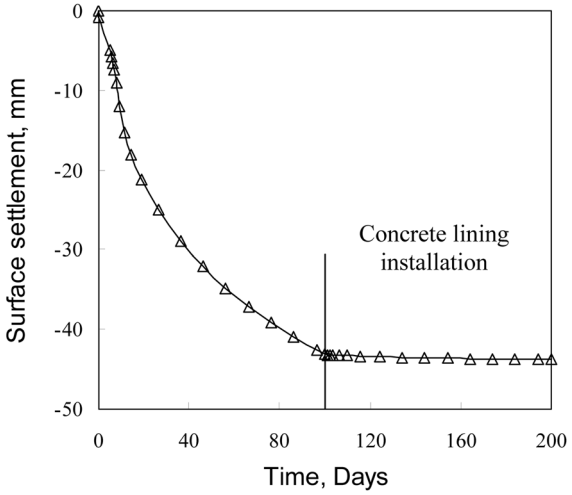

Fig. 24 Maximum surface settlement versus time relation in Case 2, where restraint of nodal displacements at periphery of tunnel occurred at 100 days after the TF advanced beyond the instrumentation line

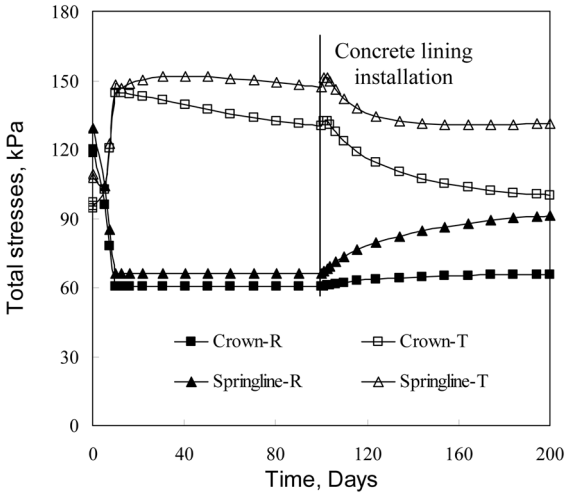

Fig. 25 Total stresses versus time relations at crown and springline in Case 2, where restraint of nodal displacements at tunnel periphery occurred at 100 days after the TF advanced beyond the instrumentation line

shallow tunnels under $K_o < 1$ predicted by Wong and Kaiser (1991). The initiation of creep zone occurs at the sidewall, and the creep zone grows outward with further stress relief. Due to the gravity effect above the shallow tunnel, the stress concentration is more severe at the tunnel shoulder so that the localized creep zone will migrate upward toward the free surface. The final configuration of the localized creep zone governs the shape of the surface settlement trough. Steeper creep zone will result in narrower settlement troughs.

The installation of permanent rigid concrete lining was simulated by restraining the displacements of the nodes at the tunnel periphery in Case 2. At the same time, the groundwater was not allowed to drain into the tunnel. Fig. 24 shows the maximum surface settlement versus time relation obtained in Case 2. The surface settlements cease after the installation of the rigid lining. Fig. 25 shows the changes of total radial and tangential stresses at the crown and sidewall during the excavation and after the permanent lining installation. The total radial stresses at both the crown and sidewall start to increase after the installation of concrete lining. However, the total tangential stress at the crown starts to decrease after the installation of concrete lining, while that at the springline increases slightly. All these total stresses start to creep back to their initial in-situ values due to the combined effect of stress relaxation and groundwater table restoration. It is of interest to notice that the settlements cease after the concrete lining installation, but the stress redistribution around the tunnel still continues to develop with time.

7. Conclusions

Numerical simulation was conducted to history match the field measurements during the construction of Shepard tunnel in clay till. The findings of this study are:

1. The excavation method and the primary lining system used in Shepard tunnel construction can be approximately simulated by 50% ground stress relief with a stress relief rate of 5%/day and partially permeable drainage boundary at the tunnel periphery.
2. Creep behaviour of the till plays an important role in quantifying the long-term settlements above Shepard tunnel. The surface settlements due to ground stress relief, consolidation and creep are 7.4, 5.3 and 31.0 mm, *i.e.*, 17, 12 and 71% of total settlement, respectively.
3. The ground settlements above the tunnel ceases after the installation of concrete lining. Therefore, when the control of ground settlements is the primary concern for tunnel construction, early installation of concrete lining could be an effective means to alleviate the concern.

Acknowledgements

This study was made possible with financial supports from Natural Sciences and Engineering Research Council of Canada and Department of Civil Engineering, The University of Calgary.

References

ABAQUS (2006), *ABAQUS Documentation*, version 6.6. ABAQUS, Inc.

Adams, K., Osborn, G., Heinz, H. and Woytiuk, M. (2008), "Origin of hummocky moraine in the Calgary area, Alberta, Canada", *Poster on Cordilleran Section (104th Annual) and Rocky Mountain Section (60th Annual) Joint Meeting*, Geological Society of America, Las Vegas, Nevada, USA.

Fredlund, D.G. and Rahardjo, H. (1993), *Soil mechanics for unsaturated soils*, John Wiley & Sons, Inc, New Jersey.

Fredlund, D.G. and Xing, A. (2004), "Equations for the soil-water characteristic curve", *Can. Geotech. J.*, **31**(3), 521-532.

Heinz, H., Woytiuk, M., Lavalley, D. and Kidd, R. (2008), "Settlement above a hand-mined tunnel in Calgary, Alberta", *Proceedings of 20th Canadian Tunnelling Conference*, Niagara Falls, Canada, October 26-28, 2008, 79-88.

Karakus, M. and Fowell, R.J. (2003), "Effects of different tunnel face advance excavation on the settlement by FEM", *Tunn. Undergr. Sp. Tech.*, **18**(5), 513-523.

Lade, P.V. and Liu, C.T. (1998), "Experimental study of drained creep behavior of sand", *J. Eng. Mech.*, **124**(8), 912-920.

Lee, K.M. and Rowe, R.K. (1991), "An analysis of three-dimensional ground movements: the Thunder Bay tunnel", *Can. Geotech. J.*, **28**(1), 25-41.

Mair, R.J. (2008), "Tunnelling and geotechnics: new horizons", *Geotech.*, **58**(9), 695-736.

Moran, S.R. (1986), "Surficial geology of the Calgary urban area", Alberta Research Council, *Bulletin 53*.

Peck, R.B. (1969), "Deep excavations and tunneling in soft ground", *Proceedings of 7th International Conference on Soil Mechanics and Foundation Engineering*, State-of-the-Art Volume, 225-290.

Shin, J.H., Addenbrooke, T.I. and Potts, D.M. (2002), "A numerical study of the effect of groundwater movement on long-term tunnel behaviour", *Geotech.*, **52**(6), 391-403.

Shin, J.H. and Potts, D.M. (2003), "Time-based two dimensional modelling of NATM tunnelling", *Can. Geotech. J.*, **39**(3), 710-724.

Wang, Z. (2010), "Soil creep behavior - laboratory testing and numerical modelling", Ph.D. thesis, Department of Civil Engineering, University of Calgary, Calgary, Alberta, Canada.

Wong, R.C.K. and Kaiser, P.K. (1991), "Performance assessment of tunnels in cohensionless soils", *J. Geotech. Eng.*, **117**(12), 1880-1901.

Wongsaroj, J., Soga, K. and Mair, R.J. (2007), "Modelling of long-term ground response to tunnelling under St James's Park, London", *Geotech.*, **57**(1), 75-90.

Woytiuk, M. (2008), "Numerical simulation of surface deformation above a shallow tunnel", MEng project report, Department of Civil Engineering, University of Calgary, Calgary, Alberta, Canada.

Woytiuk, M., Heinz, H. and Kidd, R. (2008), "Hand-mined tunnel crossing of a railway in clay till", *Proceedings of GeoEdmonton 08*, 1202-1206.

CC